# UC Davis

## UC Davis Previously Published Works

**Title**

Amphiphilic and amphoteric aqueous soy protein colloids and their cohesion and adhesion to cellulose

**Permalink**

https://escholarship.org/uc/item/3x82m2kb

**Authors**

Liu, Xingchen
Hsieh, You-Lo

**Publication Date**

2020-02-01

**DOI**

10.1016/j.indcrop.2019.112041

Peer reviewed

ELSEVIER

INDUSTRIAL CROPS AND PRODUCTS

# Amphiphilic and amphoteric aqueous soy protein colloids and their cohesion and adhesion to cellulose

Xingchen Liu, You-Lo Hsieh*

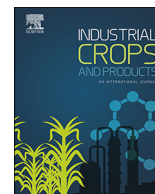*Biological and Agricultural Engineering, University of California, Davis, California, 95616, United States*

ABSTRACT

Highly stable aq. soy protein (SP) colloids have been facilely prepared by high-speed blending (30k rpm, 15 min) to homogeneously disperse up to 97.7 % of soy protein isolate at up to 9 %. Aq. SP colloids were amphoteric with a 4.5 isoelectric point and ζ-potentials ranging from $+32.4$ mV at pH 2.2 to -39.1 mV at pH 7.1 with respective average hydrodynamic diameters of 157 and 233 nm. Diluted aq. SP colloids (0.0001 %) dried on hydrophilic mica appeared as 6.0 nm thick and 16.4 nm wide disk-like nanoparticulates. Aq. SP colloids were also amphiphilic, reducing water surface tension to 41.2 mN/m at $\geq$ 0.98 % and could be solvent-exchanged to dimethyl formaldehyde or 4:1 v/v methanol/water. Colloidal SPs exhibited preferential affinity and adhesion to cellulose filter paper to significantly improve the respective tensile modulus and strength by 70 and 42 % at merely 2.8 % dried add-on. The improved cohesion of 6.2 % SPs was evident by drying at 110 °C to further increase the respective tensile modulus and strength of cellulose by another 78 and 41 %.

## 1. Introduction

Soy proteins (SPs) constitute 44–48 % of soybean meals, the major byproduct from processing soybean oil for the largest edible oil and biodiesel production in US (Canakci and Van Gerpen, 2003). Effort to utilize SPs has mainly concentrated on food product development due to their excellent nutritional values and versatile foaming, gelation and film-forming properties but very little on nonfood industrial applcations (Fukushima, 2001; Kinsella, 1979). The major hindrance to SP utilization is their poor dispersibility in water and common organic solvents, stemming mainly from their high molecular weights and globular structures. SPs contain four protein fractions of 2S, 7S, 11S and 15S of which glycinin (11S, 350 kDa, PI: 6.4) and β-conglycinin (7S, 180-210 kDa, PI: 4.8) account for the majority at 52 and 35 %, respectively (Nishinari et al., 2014). The larger glycinin is less polar, consisting 64 mol % non-polar amino acids (AAs), whereas the smaller β-conglycinin is more polar with 64 mol % polar AAs. These two SP fractions are among the largest of plant proteins, e.g., much larger than zein (19-26 kDa) and wheat gluten (25-130 kDa), and more comparable to animal proteins, such as collagen (300 kDa) and silk (250-450 kDa) (Reddy and Yang, 2011). Even though the globular structure helps to minimize the exposure of hydrophobic side groups at their surfaces or interface with water (Riblett et al., 2001), the larger and less polar glycinin is only moderately dispersible in water (Molina et al., 2001).

To better disperse SPs in water, attempts have included inducing either positive or negative charges to increase repulsive forces by adjusting pH, denaturing by heating or adding denaturants (i.e. 6 M urea or guanidinium chloride) (Guan et al., 2010; Petruccelli and Añón, 1994), adjusting ionic strength to decrease electrostatic attractions (Shen, 1981), and adding surfactants to associate with either hydrophilic or hydrophobic moieties (Malhotra and Coupland, 2004). Others have focused on molecular weight reduction by either acid (Matsudomi et al., 1985; Arboleda et al., 2014a) or enzymatic (Achouri et al., 1998; Molina Ortiz and Wagner, 2002; Chen et al., 2011a, b) hydrolysis to disperse up to 10 wt % SP hydrolysates in water (Arboleda et al., 2014a). Mechanical approaches, such as high-intensity ultrasound (20 kHz, 20 min) (Morales et al., 2015), high-pressure homogenization (207 MPa, 30 pass) (Song et al., 2013), high shear homogenization (16k rpm, 30 min) (Bi et al., 2014), and high shear microfluidization (159 MPa, 26 pass) (Jong, 2013), have also been effective to reduce the particle sizes but none could process the majority of SPs into colloids. Even the optimal high-pressure homogenization still required prior sonication (20 W, 30 min) to reduce the Z-average hydrodynamic diameter ($D_Z$) of particles from 3331 to 136 nm with a ζ-potential of $-25$ mV (Song et al., 2013), implying the incipient instability. While commercially processed SPs, such as soy protein concentrate (SPC) or isolate (SPI), are partially denatured thus less water dispersible (Wagner et al., 2000), ultrasonication of SPI and homogenization of

---

* Corresponding author.
  *E-mail address:* ylhsieh@ucdavis.edu (Y.-L. Hsieh).

SPC have shown to improve their emulsifying and foaming properties by exposing more surface hydrophobic moieties. Charged SP nanoparticles or nano-aggregates have been synthesized with thermal ($D_Z$ = 88 nm, -24 mV (Liu and Tang, 2013)) and/or chemical (glutaraldehyde and alkali) (i.e. $D_Z$ = 101 or 146 nm, -10.3 or -9.5 mV (Zhang et al., 2012); $D_Z$ = 202 nm, -36.8 mV (Teng et al., 2012)) input to be effective Pickering emulsifiers (Liu and Tang, 2013) or drug/nutrient carrier (Zhang et al., 2012; Teng et al., 2012). Questions remain if mechanical processes can convert unmodified or commercially processed SPs into stable and high concentration colloids and if colloidal SPs may serve as Pickering emulsifiers.

This work explores the use of high-speed blending shear force to process aqueous (aq.) SPI suspensions into stable colloids without additional chemical input. Blending at 30k rpm raises the temperature of aq. SPI suspensions, e.g., to ca. 87 °C after 15 min, exceeding or close to the denaturation temperatures of the two major SP globulins (7S: 74 °C; 11S: 90 °C (Nishinari et al., 2014)). The combination of shear force and heat generated in blending could potentially interrupt the non-covalent inter- and intra-molecular bonding and reduce the association of SPs. Therefore, if and to what extent high-speed blending of SPI could produce stable colloids with reduced particulate sizes and surface-active behaviors were systematically evaluated by various particulate size and surface tension characterization. As natural polyampholytes, the amphoterism of SPs was also verified by $\zeta$- potential measurements and isoelectric point determination. While SPs have served as cobinder (Erickson, 2015) and sizing (Arboleda et al., 2014b; Fahmy et al., 2010) for paper and cotton yarns (Chen et al., 2013), how colloidal SPs organize themselves in the solid forms and how they adhere to cellulose have not been reported. Hence, the structures and properties of solids dried from aq. SP colloids were studied in terms of the cohesive properties in the form of cast films and their adhesion to cellulose. With the highest nitrogen contents (17.3–17.7 %) among main plant proteins, how SPs affected the thermal properties of cellulose were analyzed.

## 2. Materials and methods

### 2.1. Materials

Soy protein isolates (SPI, 92 % proteins) were from MP Biomedicals, LLC. Regenerated cellulose dialysis membranes with 3.5 k*Da* cut-off (Fisherbrand) were used for dialysis. Hydrochloric acid (HCl, 1 N, Certified), sodium hydroxide (NaOH, 1 N, Certified), dimethylformamide (DMF, HPLC grade), methanol (MeOH, HPLC grade), ethanol (EtOH, anhydrous, histological grade), acetone (Certified), and cellulose filter paper (Whatman, Grade 4) were from Fisher Scientific and used as received. All water used was purified by Milli-Q plus water purification system (Millipore Corporate, Billerica, MA).

### 2.2. Aq. SP dispersions

Crude SPI was dispersed in water by stirring with a glass rod and dialyzed at $8 - 11$ °C for 24 h. The dialyzed aq. SPI suspensions at 1, 3, and 9 wt % were either magnetically stirred ($\sim$2k rpm, 1 h) as the control or further processed by blending at 30k rpm using a high-speed blender (Vitamix 5200) for $1 - 15$ min. Upon cooling to ambient temperature, each blended batch was centrifuged at either 5k or 14k rpm (4500 or 20,800 $g$) for 15 min to collect the supernatants or colloids for further characterization. The colloid from 15 min blending and 5k rpm centrifugation was used to compare with the control. The SP concentration was determined by drying 1 g aq. dispersion at 65 °C and weighing to calculate w/w % in triplication. All SP concentrations were in weight % and reported simply as % unless stated otherwise.

To study the dispersibility of SPs in organic solvent/water mixtures, DMF, MeOH, EtOH or acetone was added to 5 w/v % aq. control or colloids to get 1 w/v % SPs in organic solvent/water at 4:1 v/v. SPs in 4:1 v/v DMF/water were then put in a rotary evaporator under vacuum

at 35 °C for 1 h to remove water and then diluted with DMF to 1 w/v %. Foams from blending 100 g of aq. dialyzed SP dispersions at 5–9 % for 15 min were collected and weighed. Aq. dispersibility of SPs in the foam was determined by diluting it with water to completely disperse the foam and centrifuging at 14k rpm for 15 min to collect the supernatants for further characterization.

### 2.3. Characterization

#### 2.3.1. Aq. SP dispersions: light transmission, surface tension, pH, zeta potential and hydrodynamic diameter

All characterization was performed on the control or SP colloids blended at 1 % unless noted elsewhere. Light transmission of the control and colloids at 0.01, 0.1 and 1 % were measured from 400 to 800 nm using Evolution 600 UV − vis spectrophotometer (Thermo Scientific). Surface tensions (N = 5) of the control and colloids were measured over an eight order of magnitude concentration gradient by the Wilhelmy plate method using a liquid tensionmeter (K100, Kruss GmbH, Germany) at ambient temperature. The platinum plate was immersed for 3 mm and thoroughly rinsed after each measurement with water and dried under filtered compressed air stream. The isoelectric point (PI) of the colloid (25 g, 1 %) was determined by titrating with 0.1 M HCl using OAKTON pH/Con 510 series meter to derive the pH at which the second derivative was zero. The zeta ($\zeta$) potential (mV) and hydrodynamic diameter of SP particulates (N = 3) in 0.1 % colloids at pH 7.1, 6.4, and 2.2 or 0.02 % at pH 4.6 was measured with a Zetasizer Nano S90 (Malvern Instrument) at ambient temperature.

#### 2.3.2. Morphologies: AFM, TEM and SEM

SP particulates in the supernatants of the control, blended dispersions and foam dispersions were dried on mica and their heights were measured by atomic force microscopy (AFM, MFP-3D, Oxford Instruments Asylum Research, Inc., Santa Barbara, CA). Each supernatant was diluted to 0.0001 % and 10 μL was deposited onto a freshly cleaved mica surface (highest grade V1 mica discs, 15 mm, Ted Pella, Inc.) and air-dried. SP particulates were scanned in the tapping mode with OMCL-AC160TS standard silicon probes (tip radius < 10 nm, spring constant = 28.98 N/m, resonant frequency of ca. 310 kHz) (Olympus Corp.) at 1 Hz scan rate under the ambient condition. Analyses of height images were performed using Igor Pro 6.21 loaded with MFP3D 090909 + 1409 to report the average height of particulates with standard deviation (N = 150).

SP colloid at 0.0001 % were also deposited onto argon-plasma glow-discharged formvar-carbon grids (300-mesh copper, Ted Pella Inc., Redding, CA) for transmission electron microscopy (TEM, JEOL 3000, JEOL) imaging. Before the air-drying, excess liquid was removed by blotting with a filter paper after 5 min, then negatively stained with 2 % uranyl acetate solution and blotted to remove excess liquid. TEM observation was conducted at a 100-kV accelerating voltage to report the average width of 100 SP particulates with standard deviation. The surface of untreated and treated cellulose filter papers was coated with gold/palladium and imaged using a field emission scanning electron microscope (FE-SEM) (Quattro, Thermo Scientific, USA) at a $4.5 - 6$ mm working distance and 5 kV accelerating voltage.

#### 2.3.3. FTIR-ATR, XRD, thermal behavior and tensile strength

Films were cast from drying 1.5 g of 1 % control or SP colloids in polystyrene weighing boats (hexagonal side length: 1.4 cm, Fisherbrand) at 65 or 110 °C for 1 or 4 h. The secondary structure of SPs in cast films was evaluated by Fourier transform infrared attenuated total reflection (FTIR-ATR) on a Nicolet iN10 microscope spectrometer (Thermo Fisher Scientific, USA) using a liquid nitrogen cooled detector. Each spectrum was collected from 1700 to 1600 cm$^{-1}$ at a 4 cm$^{-1}$ resolution and self-deconvolution was applied based on the assumption that each narrow band within the broadened amine I was characteristic for a secondary structure (Byler and Susi, 1986). Each peak was

deconvoluted with the Levenberg − Marquardt algorithm and the peak area was curve fitted with the Gaussian function ($R^2 > 0.99$) to quantify each secondary structure component.

X-ray diffraction (XRD) patterns were also collected on films to study the crystalline structures of SPs using a Ni-filtered Cu Kα radiation ( = 1.5406 Å) with a PANalytical X'pert Pro diffractometer operated at an anode voltage of 45 kV and a current of 40 mA. Cast films were compressed between two glass slides into flat sheets with around 1 mm thickness and diffractograms were recorded from 5° to 40° at a scan rate of 2°/min. Peak deconvolution analysis was conducted using Peak Fit (Systat Software) and individual peaks were fitted by Gaussian functions with $R^2 > 0.99$ for all deconvolutions. The unit cell dimension was calculated based on Bragg's law,

$$d_{hkl} = \frac{\lambda}{2\sin\theta}$$

Thermal behaviors of cast films and SP-treated filter paper samples as well as the untreated ones were evaluated by the differential scanning calorimeter (DSC-60) and the thermogravimetric analysis (TGA-50) using a Shimadzu thermal analysis system (TA-SOWSI) at 10 °C/min heating rate under flowing $N_2$ (50 mL/min) to 500 °C and the derivative weight was derived for the derivative thermogravimetric analysis (DTG). The effects of SP colloids on tensile strength of cellulose was conducted on cellulose filter paper strips (1 cm × 7 cm, N = 5) that were immersed in water or 0.1, 0.5, and 1 wt % aq. SP colloids for 5 min, then dried at 65 or 110 °C for 1 h and conditioned at 21 °C and 65 % relative humidity for 24 h. The tensile measuremnts were made at a 40 mm gauge length and a 5 mm/min cross-head speed using an Instron tester (model 5566, Illinois Tool Works Inc., USA). The ultimate tensile stress and breaking elongation as well as the Young's modulus derived from the slope of the initial linear part of the stress-strain curves were collected and mean and standard deviation reported. A *p*-value of < 0.05 was considered as statistically significant based on Student's *t*-test.

## 3. Results and discussions

### 3.1. Aq. dispersibility

Crude SPI was magnetically stirred (∼2k rpm, 1 h) into water at up to 9 % concentrations to opaque pale-yellow suspensions that separated into one clear to translucent top layer and one opaque bottom layer (Fig. S1). The time taken to phase separate lengthened with increasing concentrations, i.e., from less than 15 min at 0.01 % and ca. 1 h at 1 %. The magnetically stirred SPs at > 9 % were paste like, thus not studied. Following centrifugation, only 23–35 % SP were found in the supernatants of originally SP dispersions (Fig. 1),showing magnetic stirring
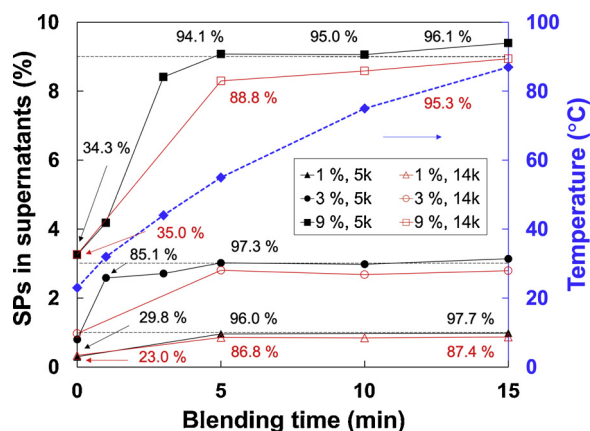


**Fig. 1.** The lengths of blending (30k rpm) time and subsequent centrifugation (5k or 14k rpm) on the extent of SPs in the supernatants of dialyzed aq. SPI dispersions at 1, 3, and 9 %.

(∼2k rpm, 1 h) to be incapable of dispersing most of the larger SPs in water.

High-speed blending (30k rpm) of 1–9 % SP suspensions for 5 min significantly improved the extents of SPs in the supernatants to 86.8–88.8 % and 94.1–97.3 % 14k and 5k rpm respectively (Fig. 1). Extending blending from 5 to 15 min dispersed 6.5 % more SPs in the supernatants (14k rpm) of the 9 % suspension. Clearly, the brief 5-min blending was sufficient to effectively disperse the majority of SPs in the supernatants. In fact, even a shorter time of 1 min could disperse 85.1 % SPs in supernatants (5k rpm) from the 3 % suspensions. Irrespective of SP concentrations, blending raised the aq. SP dispersion temperatures from 23 °C to ca. 32, 44, 55, 75, and 87 °C after 1, 3, 5, 10, and 15 min, respectively. While elevated temperatures from longer blending caused water evaporation and slightly raised the SP concentrations in some supernatants to above the original, the high proportions of SPs dispersed by short 1 or 3 min blending, both at moderate temperatures, suggested the shear force to be the dominant factor to interrupt SPs for better aqueous dispersions. Furthermore, SPs in the supernatants were lowered at 14 rpm, but the extents are small considering the nearly four times in centrifugal force. Therefore, the more energy efficient 5k rpm centrifugation was deem appropriate for preparing supernatants or colloid. With moderate 5 rpm centrifugation, high-speed blending (30k rpm) has shown to be highly effective in dispersing 94.1 % SPs from 9 % suspension after brief 5 min or 85.1 % SPs from 3 % after only 1 min, both at slightly elevated temperatures of 55 and 32 °C, respectively.

### 3.2. Light transmittance

The effect of blending was visible and clearly indicated by the transmission of visible light. The 0.01 and 0.1 % controls showed visible particles (Fig. 2a) that fully settled within 15 min. In contrast, the blended (15 min, 1 %) supernatants (5k rpm), containing 97.7 % of original SPs, appeared clear when diluted to 0.01 % (Fig. 2a). At 0.1 and 1 %, both the control and blended supernatants were bluish, suggesting the scattering of blue light by the particles. A single-wavelength light beam (λ = 638 nm) passed through 0.01 and 1 % blended supernatants uniformly (Fig. 2b), implying relatively uniform SP particulate sizes. At 1 %, the control did not transmit any visible light whereas the blended supernatant transmitted a slight 3.0 % at 400 nm and much higher 74.8 % at 800 nm (Fig. 2c-d), corresponding to its translucent appearance. Blending further increased visible light transmission of less concentrated SP supernatants to, i.e., 67.3 % and 99.6 % of the 0.1 %, and to 95.6–100 % of the 0.01 % at 400–800 nm, respectively (Fig. 2c-d). All SP supernatants, irrespective of blending time, concentrations (1, 3 or 9 %) or centrifugation levels (5k or 14k rpm), appeared similarly even upon additional centrifugation (5k rpm) under refrigeration (8 − 11 °C) for at least two weeks, showing the superior colloidal stability.

### 3.3. Dimensions of SP nanoparticulates in supernatants

The increased light transmittance of the blended supernatants was indicative of smaller SP particulates that were verified by AFM imaging of diluted supernatants at 0.0001 % air-dried on mica. The SP particulates were round and averaged in ≤ 6 nm heights that reduced with longer blending time (Fig. 3a-c, S2). The SP nanoparticulates in the supernatant (14k rpm) of the 1 % control were 2.1 ± 4.7 nm in height (Fig. 3a, S2), but only accounted for 23 % of the original SPI. Blending for 5 min reduced most of the rest SPs to be sufficiently small, i.e., average 4.6 ± 5.6 nm, to remain in the supernatant to 86.8 % (14k rpm). While tripling the blending time to 15 min only slightly further increased it to 87.4 %, the average heights were lowered to 2.9 ± 4.6 nm (Fig. 3b-c, S2). Although 1 % SPs were nearly fully (97.7 %, 14k rpm) dispersed from 15 min blending, their average height (6.0 ± 8.0 nm) almost doubled of those collected from 5k rpm (Fig. 3d, g, S2), indicating the 10.3 % additional nanoparticulates from the lower
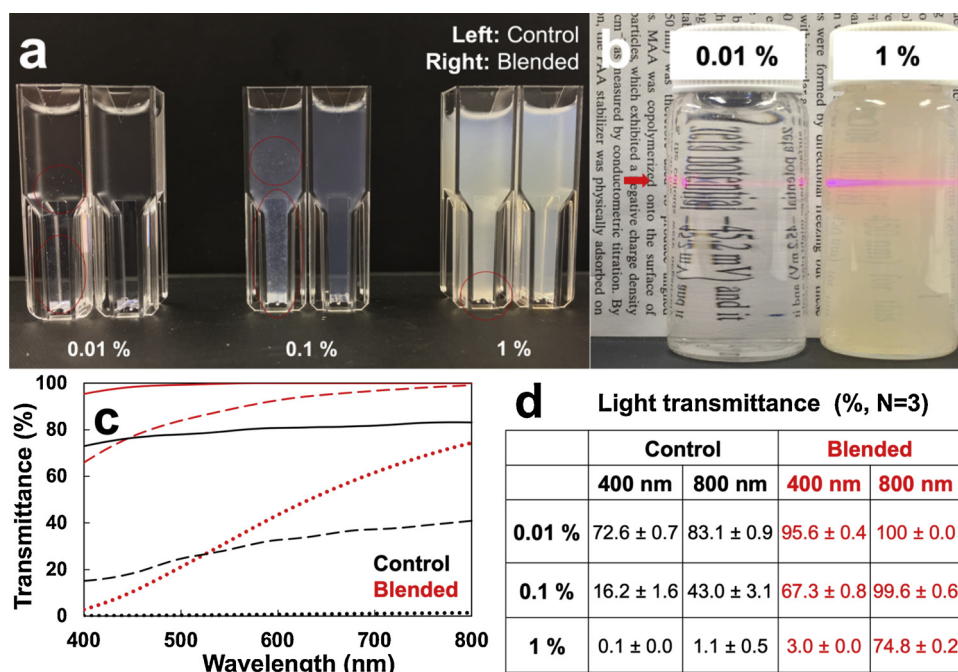
**Fig. 2.** Aq. SP control and blended (15 min) supernatants (5k rpm): (a) visual appearance, (b) single wavelength ($\lambda$ = 638 nm) light beam passing through 0.01 and 1 % blended supernatants, (c–d) visible light transmittance at 0.01, 0.1, and 1 %.

centrifugation were much larger. Blending the highest 9 % for 15 min also dispersed similarly high extent of SPs (95.3 %, 14k rpm), the nanoparticulates were ca. 2.5 times larger than those from the lowest 1 % (Fig. 3e, S2). Thus nanoparticulates collected by lower force or from higher original SP concentration contain small portions of much larger ones. But those produced from 9 % could be reduced to 3.8 nm (68 % < 3 nm) with sonication (Fig. 3f-g, S2). These results clearly validated blending to be highly efficient in dispersing SPs. While larger SP nanoparticulates remained dispersed at lower centrifugation (5k rpm), colloidal stability of supernatants was similar. Therefore, the supernatants (5k rpm) from 15 min blending at 1 and 9 % were designated as the standard colloids and further characterized and compared with the control unless noted otherwise.

Dilute (0.0001 %) supernatant from 1 % SPI dried on hydrophilic TEM grids appeared as round SP nanoparticles in varied widths from ca. 10–74 nm of which 80 % between 10 and 20 nm (Fig. 3h-j). With an average width of 16.4 nm ( ± 11.6 nm, N = 100) and an average height of 6.0 ± 8.0 nm height (Fig. 3d), SP nanoparticles were nano-disk-like. In all cases, the large standard deviations of AFM height and TEM width values may be attributed to the diverse molecular weights of different SP fractions in SPI. The larger nanoparticulates may also be clusters of SP fragments (Fig. 3i). As noted earlier, the nanoparticulates (2.1 nm in height) in the supernatant of the control, constituted 23.0 % of the original SPI, were smaller than those (2.9–6.0 nm in height) produced by blending. This proportion may correspond to the smaller 2S (8 %, 8-21.5 k*Da*) and some portions of 7S (i.e. β-amylase, 2–5 %, 61.7 k*Da*; lipoxygenase, 2 %, 102 k*Da*) (Nishinari et al., 2014) whereas blending breaks down the majority and much larger glycinin (350 k*Da*, 52 %) and β-conglycinin (180-210 k*Da*, 35 %).

### 3.4. Amphiphilicity: surface tension, foaming and dispersibility in organic liquids

Both aq. control and colloids at 0.01–1 % formed concaved meniscus inside hydrophobic polystyrene cuvettes (Fig. 2a), indicative of the amphiphic nature of SP particulates. Both also reduced the surface tension of water at 0.0001 % onset concentration (Fig. 4), with the colloid lowering the surface tension slightly more than the control (41.2

vs. 43.2 mN/m) but having a much lower critical aggregation concentration (CAC) of 0.98 % or 0.035 mM than the control (1.35 % or 0.048 mM) assuming a 280 k*Da* molecular weight for SPI (Nishinari et al., 2014). Although particulates in supernatants of the control were 2.1 nm in heights on average (Fig. 3a), the whole uncentrifuged control contained very large and visible particles. In contrast, the colloids contained all nanoparticulates with 6 nm average height and 51 % less than 3 nm (Fig. 3d, g). The much lower CAC of SP colloids is attributed to the overall smaller particulates as smaller ones are favored for adsorptions at the interface to give a lower ΔG° (Rosen and Kunjappu, 2012). The little difference in their surface tensions implied the similar proportion of the hydrophilic and hydrophobic moieties on their surfaces despite of their size difference. Overall, the far smaller SP particulates in the colloid were more surface-active and stable to function as Pickering emulsifiers. Based on the reported CAC determined by surface tension measurement, the surfactant-like behavior of pristine colloidal SPs (41.2 mN/m, 0.98 % or 0.035 mM) was found to be comparable (Bhairi, 2001; Košíková et al., 2000) or even better (Prochaska et al., 2007; Tang et al., 2014; Azzam et al., 2010 than some commercial synthetic surfactants, such as anionic sodium dodecyl sulfate (SDS, 38.5 mN/m, 0.23 % or 8 mM) and non-ionic Triton X-100 (30 mN/m, 0.014 % or 0.22 mM) (Bhairi, 2001), and chemically modified Pickering emulsifiers derived from biopolymers, such as hypochlorite-modified starch (55 mN/m, ca. 0.1 mM) (Prochaska et al., 2007), poly[2-(dimethylamino) ethyl methacrylate]-grafted cellulose nanocrystals (47 mN/m, 1 %) (Tang et al., 2014), Jeffamine-grafted cellulose nanocrystals (36–46 mN/m, ca. 1 %) (Azzam et al., 2010), and pre-hydrolyzed and lauryl bromide-modified lignin (40 mN/m, 0.0084-0.0119 w/v %) (Košíková et al., 2000).

Blending aq. SPI dispersions caused foaming at all concentrations and lengths of blending time and foams persisted for at least 1 h. Foams collected from blending 100 g of 5, 6, 7, and 9 % aq. SPI dispersions weighed 4.3, 6.6, 8.7, and 10.8 g, respectively. The similar proportion of foams generated at varied concentrations implied that a certain portion of SPs may be more prone to foaming. SP particulates in the foam had lower heights (2.7 ± 4.1 nm, Fig. S3) than those in the whole colloid (3.8 ± 5.3 nm) (Fig. 3f), suggesting those prone to foaming to be lower in molecular weights. SP particulates in the foams were 88.1 %
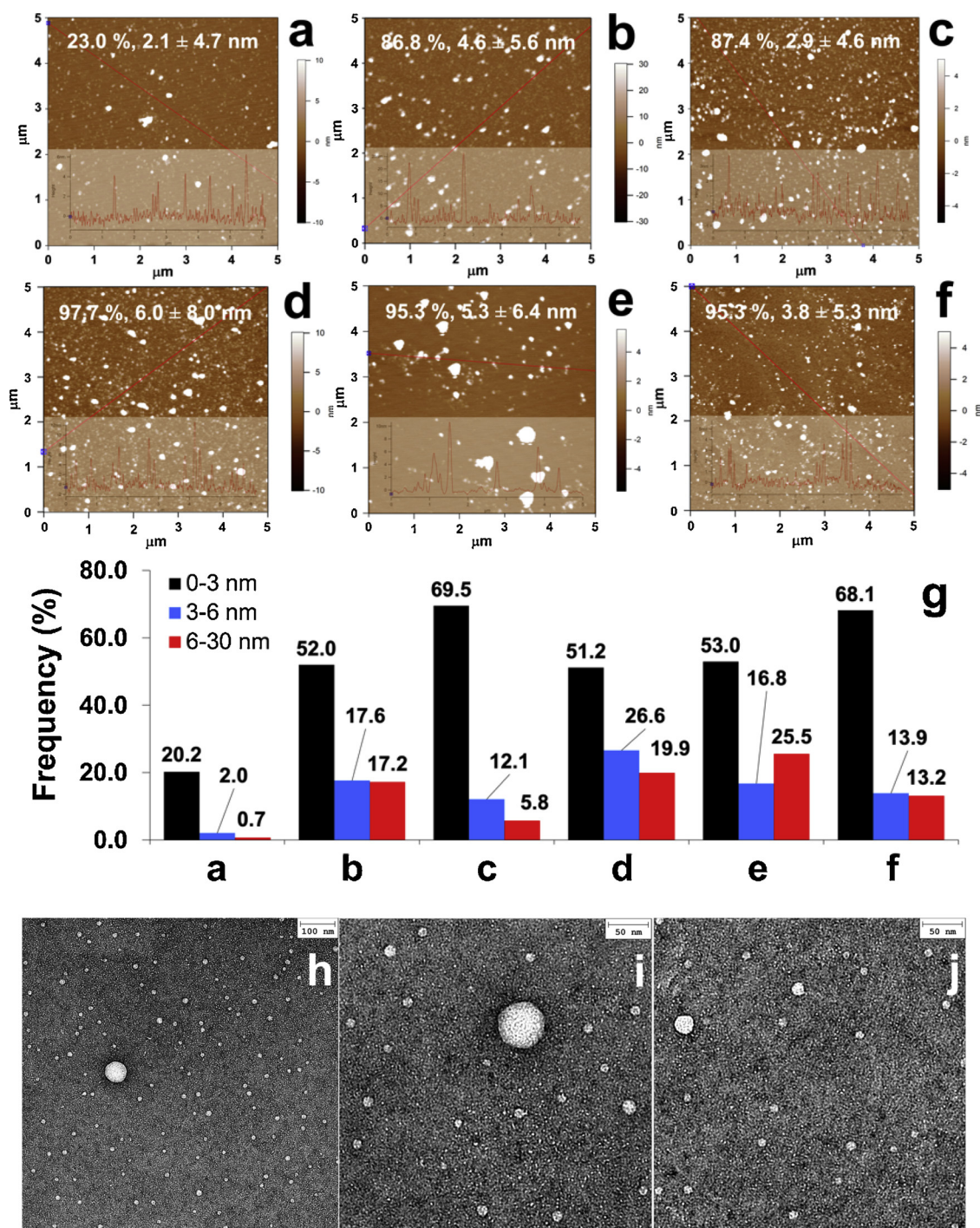
**Fig. 3.** AFM height images and profiles of SP nanoparticulates (0.0001 %) in the supernatants (14k rpm, 15 min unless noted otherwise) from blending 1 % aq. suspensions for varying lengths of time: (a) control; (b) 5 min, (c) 15 min; (d) 15 min and 5k rpm; (e) 9 %, 15 min blending; (f) e following sonication (130 W, 15 min). Values in height images denote % SPs in the supernatants and those in height profile denote means and standard deviations of heights; (g) height distributions of SP nanoparticulates in a–f (N = 150); (h–j) TEM of d.

redispersible (supernatants from 14k rpm), but less than the 95.3 % in the original colloid and tended to associate with each other (Fig. S3), suggesting those in the foams may be more hydrophobic than those in the aq. colloids. SP particulates in the foams exhibited the similar surfactant behavior with a slightly higher surface tension of 42.5 mN/m and CAC of 1.02 % (Fig. S4) than the whole colloid (41.2 mN/m, 0.98 %) (Fig. 4). Further blending of the aq. colloid also generated more foams, suggesting smaller and slightly more surface-active SP fragments may be continuously generated.

Aq. SP colloids could be solvent-exchanged into either DMF or 4:1

v/v MeOH/water at 1 w/v % as translucent and homogeneous dispersions of which less than 5 % precipitated from centrifugation (5k rpm). The SP particulates in the DMF supernatant also appeared round with a height of 5.4 ± 5.6 nm (Fig. S5), similar to those in the aq. colloid (6.0 ± 8.0 nm). When exchanged into even less polar liquids, SP particulates phase separated in 4:1 v/v EtOH/water in hours but immediately in 4:1 v/v acetone/water. Such solvent compatibility in less polar DMF and 4:1 v/v MeOH/water was observed for the first time to the best of our knowledge, greatly expanding the potential of processing SPs in organic environment and incorporating SPs with more
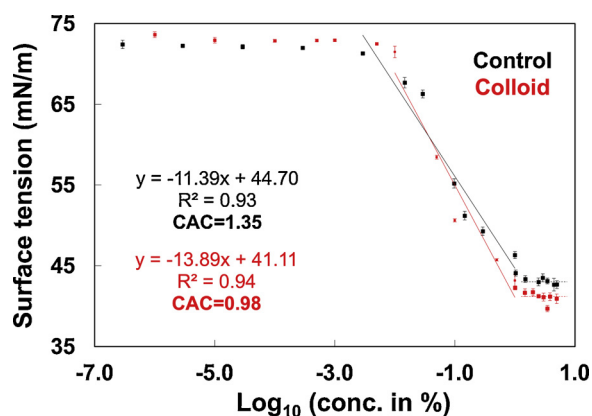
**Fig. 4.** Surface tensions of aq. SP control and colloids over the concentration gradient (N = 5).

organic compounds and polymers. Amphiphilic SP colloidal particulates facilely derived from a completely green aqueous process without involving any extra chemicals are unique Pickering emulsifiers and particularly suitable for food, pharmaceutical and cosmetic formulations, which are to be further studied.

### 3.5. Amphoterism: isoelectric point, hydrodynamic dimension and zeta potential

The isoelectric point (PI) of aq. SP colloids was determined to be 4.5 from the second derivative of the titration curve of 1 % aq. colloids with 0.1 M HCl (Fig. 5a). This PI value is within the range (4.4–4.6) reported for SPI in the literature (Malhotra and Coupland, 2004). The hydrodynamic dimensions and ζ-potentials of SP particulates were characterized using 0.1 % aq. SP, below the CAC, that appeared bluish and translucent at pH 7.1. The Z-average hydrodynamic diameter ($D_Z$) of SP particulates was 157.1 nm, one magnitude larger than the averaged width (16.4 $\pm$ 11.6 nm) of air-dried particulates on mica observed by TEM, but similar to the optimal hydrodynamic size reported by high-pressure homogenization (136 nm) (Song et al., 2013), but smaller than those by high shear homogenization (331 nm) (Bi et al., 2014) and high shear microfluidization (172 − 264 nm) (Jong, 2013), although the yield or the proportion of such particulates was not reported in these prior works. The measured ζ-potential of -39.1 $\pm$ 0.8 mV (Fig. 5b) not only indicated negatively charged nature of SP particulates at nearly neutral pH or above the PI but also implied fairly good colloidal stability (Riddick, 1968). The aq. colloidal stability observed earlier was thus attributed to not only the substantially reduced particulates size but also the repulsive forces induced by the negative surface charges at neutral pH. As the pH decreased to 6.4, turbidity evidently increased as the Z-average also slightly rose to 176.5 nm while the ζ-potential slightly reduced (-36.4 $\pm$ 0.7 mV), lowering the inter-particulate repulsive forces and increasing associations. At pH 4.6, the ζ-potential

was considerably lowered to -11.4 $\pm$ 0.6 mV and the average hydrodynamic diameter of SP particulates was significantly increased to as large as 6,942 nm, showing clear phase-separation and the lowest aq. dispersibility due to the low net charges at near PI. Further lowering the pH to 2.2 by adding in total ca. 4.5 ml 0.1 M HCl, the dispersion became more homogeneous again, consistent with the reduced hydrodynamic size to 233.1 nm. And a 34.3 $\pm$ 0.3 mV ζ-potential was measured, corresponding to protonation of the –$NH_2$ and $-COO^-$ groups into –$NH_3^+$ and $-COOH$ thus the positively charge. SPs are amphoteric polyelectrolytes based on their overall amino acid composition, i.e., 20.5 mol % acidic and 18.0 mol % basic side groups (Riblett et al., 2001). These ζ- potential behaviors show SP colloidal particulates to be amphoteric as well and their surface charges could be simply tuned by adjusting pH to be positive by protonation or negative by deprotonation.

### 3.6. Cohesion and adhesion of SP colloidal nanoparticulates to cellulose

Aq. colloids and the control suspension, both at 1 %, could be cast into pale-yellow freestanding films, with that from the colloid appearing glossier and more transparent (Fig. S6), likely due to the significantly reduced SP particulate sizes. Both films were brittle and broke easily when bended or flattened but became gel-like when submerged in water and remained intact and strong to be picked up even after 24 h (Fig. S7), then returned to similar translucent appearance and brittleness when air-dried. The resolved FTIR amide I peak showed both films to contain similarly high proportions (81.4 %, control; 81.7 % colloid) of ordered secondary structures that included α-helix and β-turns (Fig. 6a). However, the film cast from colloids contained 30 % α and 51 % β structures which were 17 % higher in β -turns but 17 % lower in α-helix than the control, suggesting α-helix transformation to β turns (Fig. 6a, S8). Drying at a higher 110 °C further increased β structures to 73 % or by 22 % at the expenses of respective 13 and 8 % decreases in α-helix and random coils (Fig. 6a, S8). The XRDs showed two major characteristic peaks at $2\theta$ = 15.9–18.9° and 22.1–30.8° and one minor peak at 8.4–9.3° (Fig. 6b, Table S1). And their corresponding D-spacings of 4.7–5.6 Å and 2.9–4.0 Å were assigned to the inner strand distance within α-helical and β-structures, respectively, and the equatorial reflection of 9.5–10.5 Å is thought to be correlated to the inter-sheet or -helix spacing as reported previously (Rama and Gupta, 1992). The crystalline index (CrI) values of films prepared from the colloid at 65 °C were 72 %, 10 % higher than the control, with more β structures and in particular doubled β turns (Fig. 6b, Table S1). Consistent with the amide I peak analysis, drying the colloid at 110 °C further increased the CrI to 83 %, also further increased β structures and especially doubled β-sheets. All SP films were hygroscopic, absorbing similar extent of moisture for those dried at 65 °C (8.2 % for the control and 8.5 % for the colloid), and slightly less for that dried at 110 °C (7.1 %) (Fig. S9, Table S2). All three films exhibited similar TGA patterns of initial mass loss at ca. 210 °C, peak decomposition temperature ($T_{max}$) at 323-325 °C, and 60–62 % mass loss at 500 °C (Fig. S9, Table S2), indicating
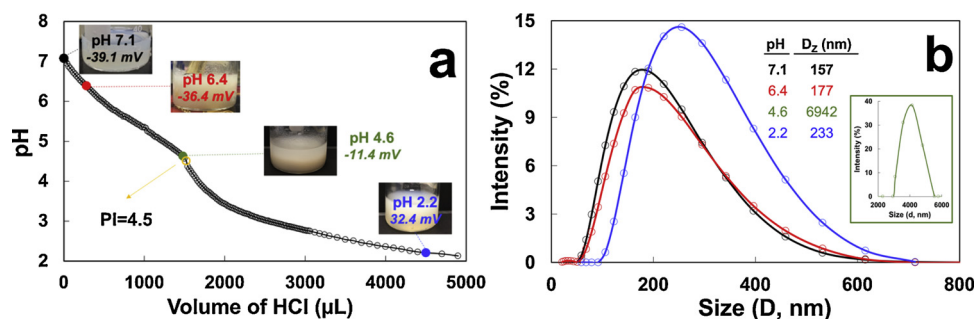


**Fig. 5.** Amphoteric characteristics of aq. SP colloids: (a) ζ-potential over pH titrated with 0.1 M HCl showing the isoelectric point (PI) at 4.5; (b) the hydrodynamic diameter distribution of SP particulates at pH 7.1, 6.4, 4.6 (inset) and 2.2 by dynamic light scattering.
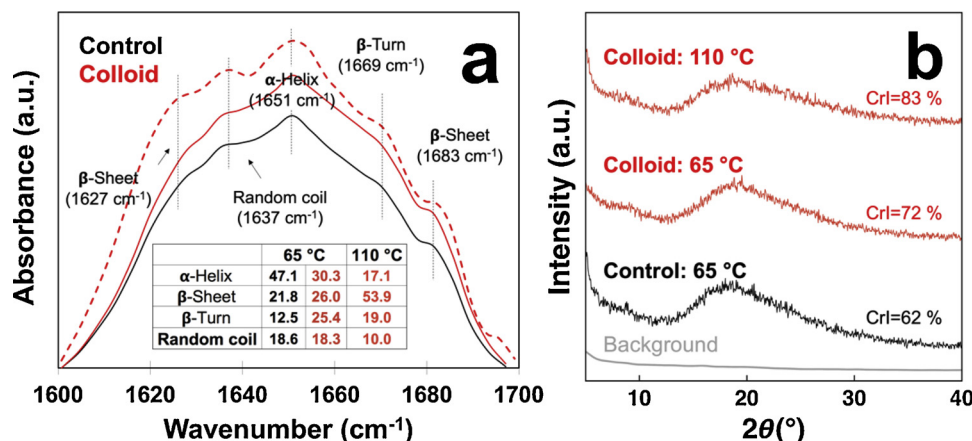
**Fig. 6.** SP films cast from the 1 % aq. control or colloid and dried at 65 (solid) or 110 °C (dash): (a) FTIR-ATR amide I region with secondary structure composition in % in the inset, (b) XRD patterns with the CrI denoted.

thermal properties unaffected by the α-helix to β-structure transformation. As aromatic (i.e. tryptophan, tyrosine, phenylalanine) and $C_β$-branched (i.e. isoleucine, valine, threonine) side groups in AAs prefer to adopt β conformations (Malkov et al., 2005), the higher β-structures in the film from aq. colloids is consistent with the fact that nearly a quarter (24 mol %) of AAs in SPs contain such hydrophobic and bulky side groups (Nishinari et al., 2014) whose secondary structural transformation appears to be facilitated by their reduced particulate sizes. Drying at 110 °C, above the denaturation temperature of all SP fractions, may interrupt and transform additional secondary structures to β-sheets.

Cellulose paper strips were immersed in aq. SP colloids at 0.1, 0.5, and 1 % concentrations, then dried at 65 or 110 °C for 1 h to study the cohesion and adhesion of SPs to cellulose. Cellulose paper absorbed 2–2.5 times of aq. SP colloids by mass, irrespective of their concentrations, and gained ca. 0.6, 2.8, and 6.2 % dry mass from 0.1, 0.5, and 1 % SP colloids, respectively. These mass gains were about three times of the values based on the liquid uptake, clearly evident of the mobility of SPs at concentrations below or near the 0.98 % CAC where they are unassociated or slightly associated and their preferential affinity to cellulose. When dried at 65 °C, the respective Young's modulus and tensile stress of the cellulose paper peaked with remarkable increases from 423 to 718 MPa (70 % increase) and from 7.4–10.5 MPa (42 % increase) at merely 2.8 % SPs, then remained similar with double amount of SPs at 6.2 % (Fig. 7a-b, Table S3). Drying at 110 °C increased the respective Young's modulus and tensile strength further to 1047 MPa and 13.3 MPa, i.e., 78 and 41 % further increases from the 2.8 % add-on dried at 65 °C, or impressively 2.5 and 1.8 times of respective modulus and strength of the untreated (Fig. 7a-b, Table S3). At comparable add-ons, the 42 % increase in tensile strength of cellulose paper with 2.8 % SPs is several times of cellulose treated with chemically modified SPI reported by others, i.e., 8 % strength increase of paper handsheets with 2.0 % hydrolyzed SPI (0.1 N HCl, 70 °C, 9 h) (Arboleda et al., 2014b) and 26.6 % strength increase with 2.5 % SPI mixed with urea and acrylamide (10:8:1) (Fahmy et al., 2010).

Both the preferential affinity of colloidal aq. SPs to cellulose surfaces and the significant tensile modulus and strength improvement with 2.8 % SPs support the dominant adhesion of SPs on cellulose, likely through H-bondings between the abundant surface polar groups of SP particulates ($-COOH$, $-NH_2$, $-OH$, and amide) and cellulose ($-OH$). The further improved tensile performance of the higher 6.2 % SPs dried at 110 °C supports the additional cohesion effect of SPs, from heat-induced dehydration and/or condensation to form covalent bonds among SP particulates, and possibly adhesion between SP and cellulose. This association between β-rich SPs with improved tensile strength of SP covered cellulose is consistent with the cohesive effect of SPs and the

rigidity of significantly dominant β structures (especially 54 % β sheets) generated at 110 °C. The only similar reinforcing effect attributed to β structure was the semi-crystalline and β-rich lysozyme amyloid fibrils on increasing the tensile modulus of polydimethylsiloxane (Oppenheim et al., 2010).

Upon heating in TGA, cellulose lost 3.4 % moisture then the majority mass sharply at above 300 °C, exhibiting $T_{max}$ at 351 °C and a peak decomposition rate of 0.65 %·$s^{-1}$ to leave 4 % char at 500 °C (Fig. 7c-d, Table S2). SP film cast at 65 °C showed gradual decomposition at above 200 °C and 30 % char (Fig. 7c-d, Table S2). The physical mixture of cellulose and 6.2 % SP cast film decomposed with similar $T_{max}$ (352 °C) and rate (0.65 %·$s^{-1}$) as cellulose, but producing 10 % char, showing the effect of SPs (Fig. 7c-d, Table S2). All SP-coated cellulose paper, regardless of the extents of SPs or drying temperatures, showed ca. 50 °C lower onset decomposition temperature, distinctively reduced peak rates (0.40-0.47 %·$s^{-1}$), and more char at 500 °C (13–15 %) (Fig. 7c-d, Table S2), supporting the adhesion and cohesion effects of SPs on cellulose. In addition, the film-like coverage of SPs on the cellulose surface (Fig. 7e-f, S10) may serve as the barrier to heat transfer to impede cellulose decomposition. Decomposed SPs, mainly as oligopeptides and/or AAs that bear carboxylic groups, may also catalyze the dehydration of cellulose towards the production of more thermally stable char (Hanna, 1984). Other proteins, such as heat-denatured whey proteins (Bosco et al., 2013), caseins (Alongi et al., 2014), and hydrophobins (Alongi et al., 2014), have also shown to lower the decomposition rates of cottons at $T_{max}$ by ca. 30–50 % and the onset decomposition temperature by 40 °C, but all at a substantially higher 20 % add-on (Bosco et al., 2013; Alongi et al., 2014). Most distinctively, SP colloids have shown similarly improved thermal stability for cotton cellulose paper, i.e. reduced decomposition rate by about a third and increased char by more than three times, but at a much lower 2.8 or 6.2 % add-on.

## 4. Conclusion

High-speed blending (30k rpm) has shown to facilely process the easily phase-separated aq. suspensions of commercial soy protein isolate (SPI) into highly stable aqueous SP colloids at up to 9 % and in high yields (up to 97.7 %). Optimally processed (30k rpm, 15 min) aq. SP colloids (5 k rpm centrifugation) appeared clear (0.01 %) to translucent (1 %), contained 157.1 nm average hydrodynamic diameter particulates (0.1 %), and 6.0 ± 8.0 nm thick (AFM) and 16.4 ± 11.6 nm wide (TEM) disk-like nanoparticulates when dried from diluted 0.0001 % on hydrophilic surfaces. With a PI of 4.5, colloidal SPs were amphoteric and could be deprotonated or protonated to wide ranging ζ-potentials from -39.1 mV at pH 7.1 to 32.4 mV at pH 2.2. Aq. SP colloids were also
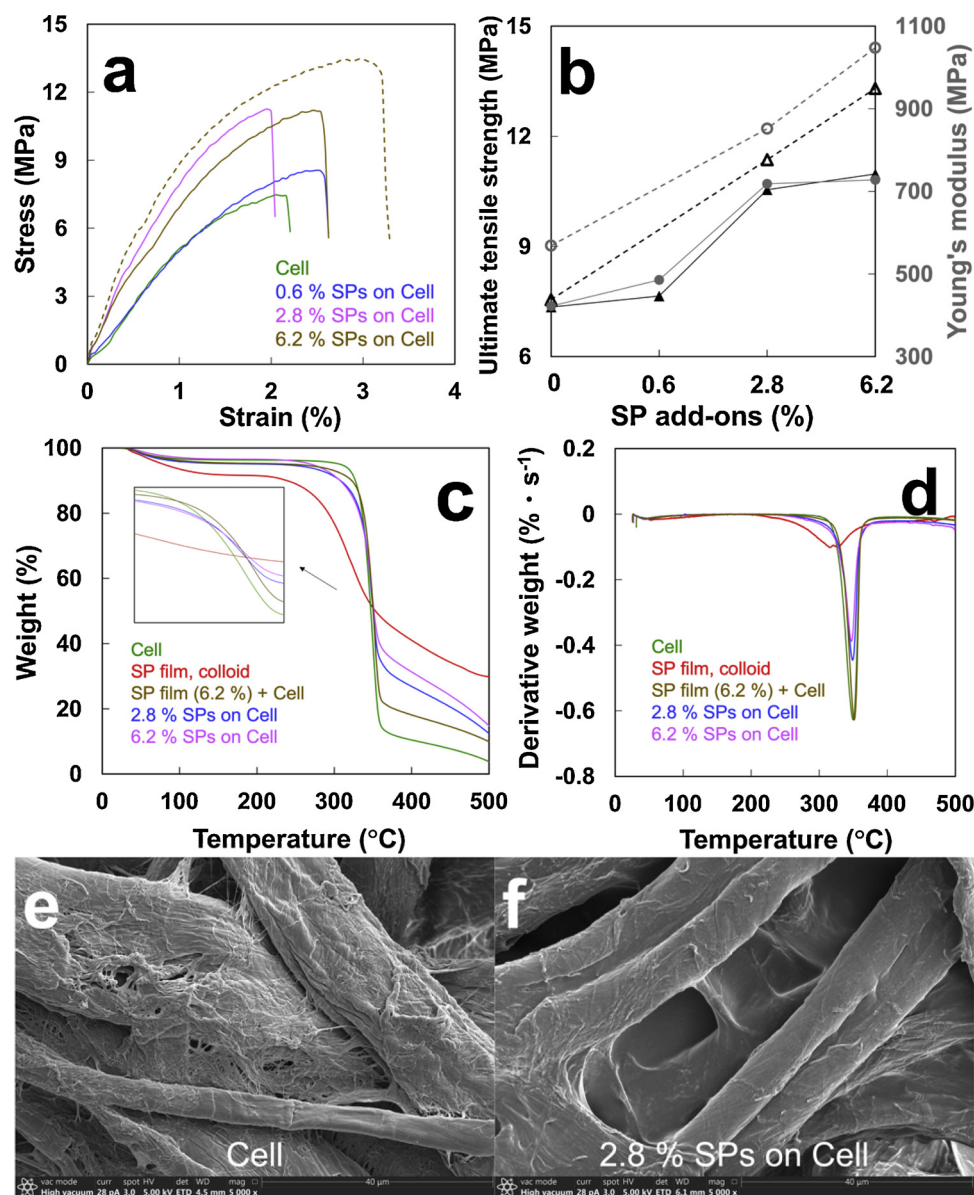
**Fig. 7.** Cellulose (Cell) filter paper with 0, 0.6, 2.8, and 6.2 % SP add-ons dried at 65 (solid) or 110 °C (dash): (a) stress-strain curves; (b) ultimate tensile strength and Young's modulus (grey); (c) TGA; (d) DTG; (e) SEM image of Cell; (f) SEM image of Cell with 2.8 % SP add-ons dried at 110 °C.

amphiphilic, capable of reducing water surface tension to 41.2 mN/m at above 0.98 % CAC, remaining colloidal when solvent-exchanged to DMF or 4:1 v/v MeOH/water, and behaving as Pickering emulsifiers. SPs in aq. colloids at up to 1 % exhibited preferential affinity and adhesion to cellulose to significantly improve the tensile modulus (70 %) and strength (42 %) of cellulose filter papers with merely 2.8 % SPs. Additional cohesive effect of SPs was evident by further tensile modulus and strength increases, by another 78 and 41 %, respectively, attributed to the enhanced hydrogen and/or new covalent bonding between SPs and cellulose by dehydration and condensation and the transformation to dominant $\beta$ structures. The thermal stability of cellulose was modestly improved by SPs, similar to other proteins but at only fractions of add-ons, signifying the capability of the colloidal form of SPs. These well documented amphiphilicity and amphoterism of aq. colloidal SP particulates are unique and the initial demonstration of their adhesive and cohesive enhancement of cellulose has broad potential applications for paper and textiles.

## Appendix A. Supplementary data

Supplementary data associated with this article can be found, in the online version, at https://doi.org/10.1016/j.indcrop.2019.112041.

## References

Canakci, M., Van Gerpen, J.H., 2003. Comparison of engine performance and emissions for petroleum diesel fuel, yellow grease biodiesel, and soybean oil biodiesel. Trans. ASAE 46 (4), 937.

Fukushima, D., 2001. Recent progress in research and technology on soybeans. Food Sci. Technol. Res. 7 (1), 8–16.

Kinsella, J.E., 1979. Functional properties of soy proteins. J. Am. Oil Chem. Soc. 56 (3), 242–258.

Nishinari, K., Fang, Y., Guo, S., Phillips, G., 2014. Soy proteins: a review on composition,

aggregation and emulsification. Food Hydrocoll. 39, 301–318.

Reddy, N., Yang, Y., 2011. Potential of plant proteins for medical applications. Trends Biotechnol. 29 (10), 490–498.

Riblett, A.L., Herald, T.J., Schmidt, K.A., Tilley, K.A., 2001. Characterization of β-con-glycinin and glycinin soy protein fractions from four selected soybean genotypes. J. Agric. Food Chem. 49 (10), 4983–4989.

Molina, E., Papadopoulou, A., Ledward, D.A., 2001. Emulsifying properties of high pressure treated soy protein isolate and 7S and 11S globulins. Food Hydrocoll. 15 (3), 263–269.

Guan, J., Porter, D., Tian, K., Shao, Z., Chen, X., 2010. Morphology and mechanical properties of soy protein scaffolds made by directional freezing. J. Appl. Polym. Sci. 118 (3), 1658–1665.

Petruccelli, S., Añón, M., 1994. Relationship between the method of obtention and the structural and functional properties of soy proteins isolates. 1. Structural and hy-dration properties. J. Agric. Food Chem. 42 (10), 2161–2169.

Shen, J.L., 1981. Solubility and viscosity. Protein Functionality in Foods Vol. 147. AMERICAN CHEMICAL SOCIETY, pp. 89–109.

Malhotra, A., Coupland, J.N., 2004. The effect of surfactants on the solubility, zeta po-tential, and viscosity of soy protein isolates. Food Hydrocoll. 18 (1), 101–108.

Matsudomi, N., Sasaki, T., Kato, A., Kobayashi, K., 1985. Conformational changes and functional properties of acid-modified soy protein. Agric. Biol. Chem. 49 (5), 1251–1256.

Arboleda, J.C., Rojas, O.J., Lucia, L.A., 2014a. Acid-generated soy protein hydrolysates and their interfacial behavior on model surfaces. Biomacromolecules 15 (11), 4336–4342.

Achouri, A., Zhang, W., Shiying, X., 1998. Enzymatic hydrolysis of soy protein isolate and effect of succinylation on the functional properties of resulting protein hydrolysates. Food Res. Int. 31 (9), 617–623.

Molina Ortiz, S.E., Wagner, J.R., 2002. Hydrolysates of native and modified soy protein isolates: structural characteristics, solubility and foaming properties. Food Res. Int. 35 (6), 511–518.

Chen, L., Chen, J., Ren, J., Zhao, M., 2011a. Effects of ultrasound pretreatment on the enzymatic hydrolysis of soy protein isolates and on the emulsifying properties of hydrolysates. J. Agric. Food Chem. 59 (6), 2600–2609.

Chen, L., Chen, J., Ren, J., Zhao, M., 2011b. Modifications of soy protein isolates using combined extrusion pre-treatment and controlled enzymatic hydrolysis for improved emulsifying properties. Food Hydrocoll. 25 (5), 887–897.

Morales, R., Martínez, K.D., Ruiz-Henestrosa, V.M.P., Pilosof, A.M., 2015. Modification of foaming properties of soy protein isolate by high ultrasound intensity: particle size effect. Ultrason. Sonochem. 26, 48–55.

Song, X., Zhou, C., Fu, F., Chen, Z., Wu, Q., 2013. Effect of high-pressure homogenization on particle size and film properties of soy protein isolate. Ind. Crops Prod. 43, 538–544.

Bi, C.-h., Li, D., Wang, L.-j., Gao, F., Adhikari, B., 2014. Effect of high shear homo-genization on rheology, microstructure and fractal dimension of acid-induced SPI gels. J. Food Eng. 126, 48–55.

Jong, L., 2013. Characterization of soy protein nanoparticles prepared by high shear microfluidization. J. Dispers. Sci. Technol. 34 (4), 469–475.

Wagner, J.R., Sorgentini, D.A., Añón, M.C., 2000. Relation between solubility and surface hydrophobicity as an indicator of modifications during preparation processes of commercial and laboratory-prepared soy protein isolates. J. Agric. Food Chem. 48 (8), 3159–3165.

Liu, F., Tang, C.-H., 2013. Soy protein nanoparticle aggregates as Pickering stabilizers for oil-in-water emulsions. J. Agric. Food Chem. 61 (37), 8888–8898.

Zhang, J., Liang, L., Tian, Z., Chen, L., Subirade, M., 2012. Preparation and in vitro evaluation of calcium-induced soy protein isolate nanoparticles and their formation mechanism study. Food Chem. 133 (2), 390–399.

Teng, Z., Luo, Y., Wang, Q., 2012. Nanoparticles synthesized from soy protein: prepara-tion, characterization, and application for nutraceutical encapsulation. J. Agric. Food Chem. 60 (10), 2712–2720.

Erickson, D.R., 2015. Practical Handbook of Soybean Processing and Utilization. Elsevier.

Arboleda, J.C., Niemi, N., Kumpunen, J., Lucia, L.A., Rojas, O.J., 2014b. Soy protein-based polyelectrolyte complexes as biobased wood fiber dry strength agents. ACS Sustain. Chem. Eng. 2 (10), 2267–2274.

Fahmy, Y., El-Wakil, N.A., El-Gendy, A.A., Abou-Zeid, R.E., Youssef, M.A., 2010. Plant proteins as binders in cellulosic paper composites. Int. J. Biol. Macromol. 47 (1), 82–85.

Chen, L., Reddy, N., Yang, Y., 2013. Soy proteins as environmentally friendly sizing agents to replace poly (vinyl alcohol). Environ. Sci. Pollut. Res. 20 (9), 6085–6095.

Byler, D.M., Susi, H., 1986. Examination of the secondary structure of proteins by de-convolved FTIR spectra. Biopolymers 25 (3), 469–487.

Rosen, M.J., Kunjappu, J.T., 2012. Surfactants and Interfacial Phenomena. John Wiley & Sons.

Bhairi, S., 2001. A guide to the properties and uses of detergents in biological systems. Calbiochem-Novabiochem.

Košíková, B., Ďuriš, M., Demianová, V., 2000. Conversion of lignin biopolymer into surface-active derivatives. Eur. Polym. J. 36 (6), 1209–1212.

Prochaska, K., Kędziora, P., Le Thanh, J., Lewandowicz, G., 2007. Surface activity of commercial food grade modified starches. Colloids Surf. B Biointerfaces 60 (2), 187–194.

Tang, J., Lee, M.F.X., Zhang, W., Zhao, B., Berry, R.M., Tam, K.C., 2014. Dual responsive pickering emulsion stabilized by poly[2-(dimethylamino)ethyl methacrylate] grafted cellulose nanocrystals. Biomacromolecules 15 (8), 3052–3060.

Azzam, F., Heux, L., Putaux, J.-L., Jean, B., 2010. Preparation By Grafting Onto, Characterization, and Properties of Thermally Responsive Polymer-Decorated Cellulose Nanocrystals. Biomacromolecules 11 (12), 3652–3659.

Riddick, T.M., 1968. Control of colloid stability through zeta potential. Blood 10 (1).

Rama, R.D., Gupta, V.B., 1992. Crystallite orientation in wool fibers. J. Appl. Polym. Sci. 46 (6), 1109–1112.

Malkov, S., Zivkovic, M.V., Beljanski, M.V., Zaric, S.D., 2005. Correlations of amino acids with secondary structure types: connection with amino acid structure. arXiv preprint q-bio/0505046.

Oppenheim, T., Knowles, T.P.J., Lacour, S.P., Welland, M.E., 2010. Fabrication and characterisation of protein fibril–elastomer composites. Acta Biomater. 6 (4), 1337–1341.

Hanna, A., 1984. The thermal degradation of cotton fibres treated with sodium hydro-xide. Acta Polym. 35 (10), 656–659.

Bosco, F., Carletto, R.A., Alongi, J., Marmo, L., Di Blasio, A., Malucelli, G., 2013. Thermal stability and flame resistance of cotton fabrics treated with whey proteins. Carbohydr. Polym. 94 (1), 372–377.

Alongi, J., Carletto, R.A., Bosco, F., Carosio, F., Di Blasio, A., Cuttica, F., Antonucci, V., Giordano, M., Malucelli, G., 2014. Caseins and hydrophobins as novel green flame retardants for cotton fabrics. Polym. Degrad. Stab. 99, 111–117.